Bed scour by debris flows: experimental investigation of effects of debris-flow composition

Tjalling de Haas[*] and Teun van Woerkom
Faculty of Geosciences, Utrecht University, 3508 TC Utrecht, The Netherlands

*Correspondence to: Tjalling de Haas, Faculty of Geosciences, Utrecht University, 3508 TC, Utrecht, The Netherlands. E-mail: t.dehaas@uu.nl

ESPL
Earth Surface Processes and Landforms

ABSTRACT: Debris flows can grow greatly in size by entrainment of bed material, enhancing their runout and hazardous impact. Here, we experimentally investigate the effects of debris-flow composition on the amount and spatial patterns of bed scour and erosion downstream of a fixed to erodible bed transition. The experimental debris flows were observed to entrain bed particles both grain by grain and en masse, and the majority of entrainment was observed to occur during passage of the flow front. The spatial bed scour patterns are highly variable, but large-scale patterns are largely similar over 22.5–35° channel slopes for debris flows of similar composition. Scour depth is generally largest slightly downstream of the fixed to erodible bed transition, except for clay-rich debris flows, which cause a relatively uniform scour pattern. The spatial variability in the scour depth decreases with increasing water, gravel (= grain size) and clay fraction. Basal scour depth increases with channel slope, flow velocity, flow depth, discharge and shear stress in our experiments, whereas there is no correlation with grain collisional stress. The strongest correlation is between basal scour and shear stress and discharge. There are substantial differences in the scour caused by different types of debris flows. In general, mean and maximum scour depths become larger with increasing water fraction and grain size, and decrease with increasing clay content. However, the erodibility of coarse-grained experimental debris flows (gravel fraction = 0.64) is similar on a wide range of channel slopes, flow depths, flow velocities, discharges and shear stresses. This probably relates to the relatively large influence of grain-collisional stress to the total bed stress in these flows (30–50%). The relative effect of grain-collisional stress is low in the other experimental debris flows (<5%), causing erosion to be largely controlled by basal shear stress. © 2016 The Authors Earth Surface Processes and Landforms Published by John Wiley & Sons Ltd.

KEYWORDS: debris flow; scour; erosion; composition; rheology

Introduction

Debris flows are common phenomena in mountainous regions on Earth and Mars (e.g. Iverson, 1997; Blair and McPherson, 2009; De Haas et al., 2015b, 2015c, 2015d). They are water-laden masses of soil and fragmented rock with volumetric sediment concentrations exceeding 40%, their maximum speeds can surpass 10 m s^{-1} and their sizes range up to 10^8 m^3 (Costa, 1988; Iverson, 1997). They typically consist of a steep front (head) containing the largest boulders and highest sediment concentration, followed by a more fluidal and turbulent slurry (tail) (e.g. Iverson, 1997). Debris flows rush down mountainsides and spill out onto valley floors and alluvial fans, where they can devastate people and property (e.g. Iverson, 2014).

Debris-flow torrents often consist of bedrock and colluvium and other types of coarse sediment. The loose sediment in these torrents can be partially to completely incorporated into the flowing mass (e.g. Hungr et al., 2005). Debris flows may grow by several orders of magnitude after initiation as they erode material along their flow path before deposition is initiated (e.g. Hungr et al., 2005; Navratil et al., 2013; Theule et al., 2015). For example, volumetric increases of 50 times the initial slide volume have been reported (Hungr et al.,

2005), as have volumetric growth rates exceeding 20 m^3 m^{-1} (Santi et al., 2008). In contrast, other debris flows have been observed to barely erode and grow in size (e.g. Pérez, 2001). An increase in debris-flow volume enhances runout distance, inundation area, flow depth and flow velocity, which increases the hazardous impact of debris flows on downstream environments (e.g. Rickenmann, 1999, 2005; Griswold and Iverson, 2008; De Haas et al., 2015a). Accordingly, a global analysis of debris flows in the period 1950–2011 shows that fatalities increase with debris-flow volume (Dowling and Santi, 2014). However, despite its ubiquity and potentially hazardous impact, the process of debris-flow erosion in general is still poorly understood, and field and experimental observations are both partly contradictory (e.g. Hungr et al., 2005; Schürch et al., 2011).

Sediment erosion by debris flows may occur when sediment is mobilized by basal shear forces (e.g. Takahashi, 1981; Hungr et al., 2005), or it may be related to grain-collisional stresses arising from the shear of the granular material (e.g. Stock and Dietrich, 2006; Hsu et al., 2008; Berger et al., 2011; Reid et al., 2011). In either case, forces on the bed are expected to be greatest at the debris flow front, where flow depth is largest and most coarse sediment is concentrated (e.g. Berger et al., 2011). Accordingly, in the Illgraben catch-

ment (Switzerland) the majority of erosion was observed to take place during the passage of the flow front (Berger *et al.*, 2011), because of the impact stresses of coarse particles recirculating at the flow front and the high basal shear stress resulting from the relatively large flow depth at the flow front. However, significant erosion at Chalk Creek (USA) was observed to occur during passage of dense granular fronts as well as during water-rich, inter-surge flow (McCoy *et al.*, 2012). As the flow transitioned from dense granular slurries to water-rich, inter-surge flow, entrainment of bed sediment continued and the measured entrainment rate did not change. Rickenmann *et al.* (2003) found that most erosion takes place behind the flow front, where the debris-flow mixture is generally more fluid in various small and large-scale experimental debris flows, suggesting that the local flow conditions at the front are not of primary importance for the erosion and entrainment of bed material. Hungr *et al.* (2005) suggest that flows with lower sediment concentrations by volume are expected to be more erosive then flows with larger sediment concentrations. In laboratory experiments, Rickenmann *et al.* (2003) found that the erosion rate initially increased with increasing volumetric sediment concentration up to 0.4, and then decreased as sediment concentration increased. However, these observations are contradictory to field observations indicating that erosion occurs mostly during passage of the granular flow front, which typically has a high coarse particle and sediment concentration (e.g. Stock and Dietrich, 2006; Berger *et al.*, 2011).

There have been very few measurements of the spatial patterns of erosion induced by debris flows, but measurements in the Illgraben torrent suggest that these patterns are highly variable and a broad range of erosion depths is possible under similar flow conditions (Schürch *et al.*, 2011). Moreover, the controls on the types of bed entrainment are poorly understood. Debris flows may entrain bed material en masse (e.g., Takahashi, 1991; Tognacca *et al.*, 2000) or through progressive downward scour (e.g. Reid *et al.*, 2011; McCoy *et al.*, 2012), but whether these processes occur together or in isolation is unknown.

Erosion can strongly influence flow dynamics, and therefore it is important to include the effects of entrainment in dynamic debris-flow models and hazard assessments (e.g. Frank *et al.*, 2015; Chen and Zhang, 2015; Iverson and Ouyang, 2015). To do so, it is important to understand which observable variables best describe erosion potential. Many such variables have been shown to positively correlate with erosion potential, including flow volume (e.g. Chen *et al.*, 2005), flow depth (e.g. Schürch *et al.*, 2011; Berger *et al.*, 2011), flow velocity (e.g. Fagents and Baloga, 2006; Iverson, 2012), discharge (e.g. Rickenmann *et al.*, 2003), bed slope (e.g. Conway *et al.*, 2010; Theule *et al.*, 2015), shear stress (e.g. Schürch *et al.*, 2011; Berger *et al.*, 2011; Han *et al.*, 2015), grain collisional stress (e.g. Hsu *et al.*, 2008, 2014; Yohannes *et al.*, 2012) and bed wetness (e.g. Reid *et al.*, 2011; Iverson *et al.*, 2011). Moreover, erosion was shown to negatively correlate with solids concentration (e.g. Hungr *et al.*, 2005). However, results are ambiguous. For example, McCoy *et al.* (2012) found that rates and occurrences of bed-sediment entrainment at Chalk Creek were not well correlated with bulk-flow properties such as density, flow depth and velocity but were dominantly controlled by bed wetness. Moreover, many of these variables are related, such as flow depth, flow velocity and discharge, and therefore it should be investigated which variables do best describe erosion potential, for future estimations and considerations of bed entrainment by debris flows, as well as for incorporation in debris-flow models.

The heterogeneous response of debris-flow erosion to various types of processes and forcings might be related to variations in debris-flow composition (i.e. grain-size distribution and water content) and rheology. De Haas *et al.* (2015a) show that debris-flow composition strongly influences flow dynamics (e.g. flow depth and flow velocity) and thus probably also their erosive potential. As such, the effects of debris-flow composition on debris-flow erodibility need to be investigated.

A relatively large amount of bed erosion in channels often occurs directly downstream of a fixed to erodible bed transition, such as downstream of bedrock channels or structures. This has been extensively investigated for streamflows (e.g. Bormann and Julien, 1991; Hoffmans and Pilarczyk, 1995), but has been hardly investigated for debris flows. Downstream of a fixed bed, erosion is often maximized because bed material that is being eroded is not replenished. Experimentally investigating bed erosion by debris flows downstream of a fixed to erodible bed transition will thus maximize the erosion signal and thereby trends between erosion and hydrodynamic and topographic forcings. Moreover, such an experimental investigation provides a first step to small-scale experimental investigation of erosion by debris flows along the entire thalweg.

This study aims to experimentally assess the effects of debris-flow composition on bed scour by debris flows at the transition from fixed to erodible bed (i.e. the bedrock–colluvium transition or downstream of structures). More specifically, we aim to (i) determine the erosive potential of various types of debris flows, (ii) evaluate which variables (out of channel slope, flow velocity, flow depth, discharge and shear stress and grain collisional stress) best predict the amount of debris-flow erosion and (iii) determine the spatial scour patterns under various types of debris flows.

The structure of this paper is as follows. First, the layout and boundary conditions of the experimental flume and laboratory experiments and the measurement and data reduction techniques are described. We present observations of the debris-flow characteristics, erosional mechanisms and spatial scour patterns. Additionally, the factors controlling erosion and the effects of debris-flow composition thereon are described. Finally, we discuss the controls on debris-flow scour and erosion, thresholds for incipient bed scour and spatial scour patterns, and elaborate briefly on the translation of the experimental results to natural systems in terms of scaling.

Materials and Methods

We evaluated basal scour depth on a dry erodible bed in a small-scale experimental flume (Figure 1), on a range of channel slopes (22.5–35°) and for eight debris-flow mixtures (Table I). In total, 86 experiments were performed (Datasets S1 and S2). To account for the effects of natural variability, each experimental setting was repeated twice.

Debris-flow composition

The debris-flow mixtures were composed of four types of sediment combined in different ratios. These were clay (kaolinite), well-sorted fine silica sand, poorly sorted coarse silica sand and basaltic gravel (2–5 mm) (cf. De Haas *et al.*, 2015a, see their Figure 3). Debris-flow composition was varied by systematically changing the amounts of angular gravel (2–5 mm), clay (kaolinite) and water fractions relative to a reference debris-flow mixture (cf. De Haas *et al.*, 2015a) (Table I and Figure 2). The total debris-flow volume was similar in all experiments. The reference sediment mixture consisted of 100 g clay, 1050 g fine sand, 2950 g coarse sand and 900 g gravel, mixed with 1500 g water. For simplicity, we refer to
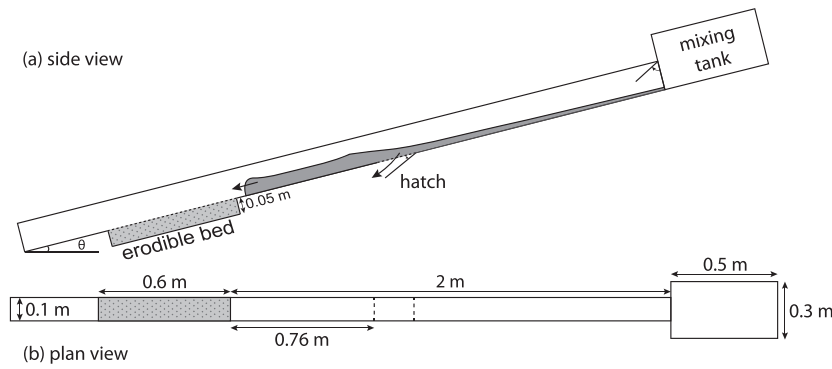
Figure 1. Experimental setup: (a) side view; (b) plan view.

Table I. Experimental debris-flow characteristics

Debris flow		Reference	water−	water+	water++	gravel+	gravel++	clay+	clay++
Gravel	vol%	18	18	18	18	40	64	16	14
Sand	vol%	80	80	80	80	59	35	73	63
Clay	vol%	2	2	2	2	1	1	11	23
Water	vol%	44	40	54	64	44	44	44	44
Volume	m³	3.4×10^{-3}	3.4×10^{-3}	3.4×10^{-3}	3.4×10^{-3}	3.4×10^{-3}	3.4×10^{-3}	3.4×10^{-3}	3.4×10^{-3}
Mass	g	6500	6750	5933	5399	6500	6500	6500	6500
Slope range	°	22.5–35	30–35	22.5–35	22.5–35	22.5–35	22.5–35	22.5–35	22.5–35

Note: See Figure 2 for detailed particle-size distributions. The gravel, sand and clay fraction are defined as the fraction within the total solids volume, and the water fraction is defined as the volume of water relative to the total debris-flow volume (solids and water). We converted mass to volume by assuming a constant solids density of 2650 kg m⁻³.
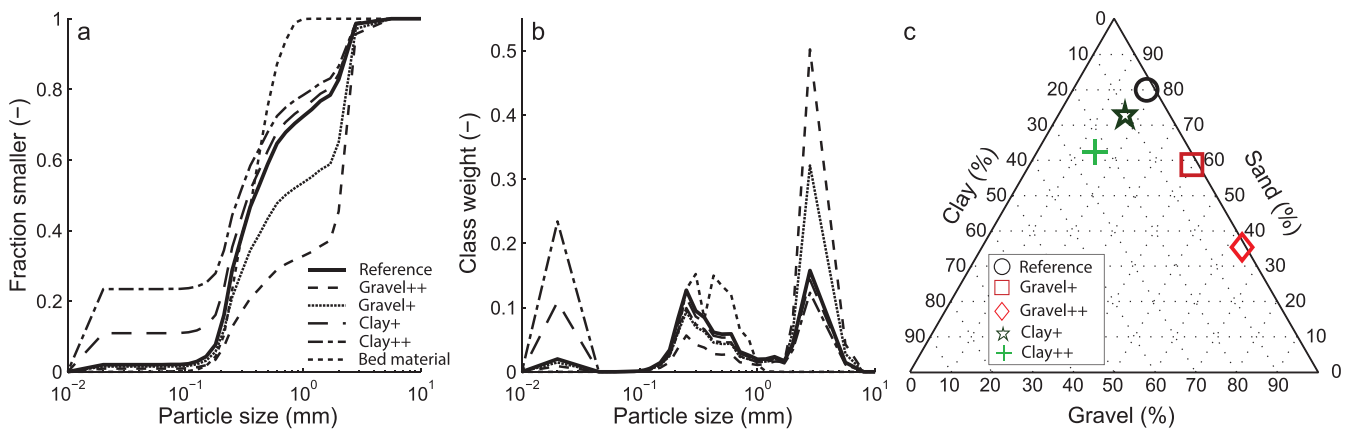

Figure 2. Sediment textures of the bed sediment and debris-flow mixtures: (a) cumulative particle-size distribution; (b) frequency distribution; (c) ternary diagram indicating the relative volumetric contribution of clay, sand (fine- and coarse-sand components combined), and gravel of the various sediment compositions used in the experiments. The sediment composition of the water−, water+ and water++ mixtures is similar to the sediment composition of the reference mixture.

the different mixtures as reference mixture, water−, water+, water++, gravel+, gravel++, clay+ and clay++; see Table I and Figure 2 for the exact composition of these mixtures. The gravel, sand and clay fractions are defined as the fraction within the total solids volume, and the water fraction as the volume of water relative to the total debris-flow volume (solids and water combined).

Experimental setup and data collection

The experimental flume consists of a straight channel with a length of 3 m and a width of 0.103 m (Figure 1) and is a slightly adjusted version of the experimental setup used in

De Haas *et al.* (2015a) and De Haas et al. (2016). The upper 2 m of the channel has a fixed bed, of which the channel bed and sidewalls are covered with sandpaper (grade 80; average particle diameter 0.19 mm) to simulate natural channel roughness. Below this reach a 0.76 m long erodible bed with a thickness of 0.05 m was present. The erodible bed thickness was larger than the maximum scour depth in all experiments, so no supply-limited erosion conditions occurred in the experiments. A hatch was present 0.76 m upstream of the fixed to erodible bed transition, which opened at a constant time interval of 1.5 s after debris-flow initiation, to divert the debris-flow tail to prevent enhanced deposition on top of the erodible bed by material transported by
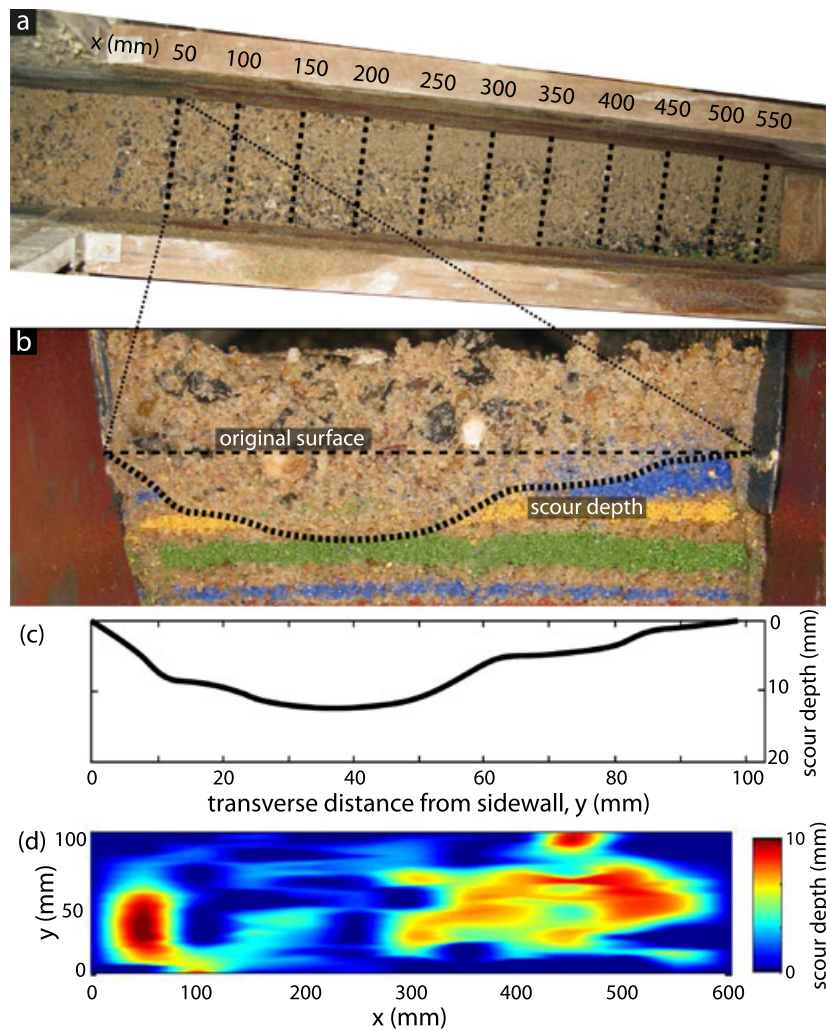
Figure 3. Methodology to reconstruct the basal scour depth map (example from experiment 004): (a) vertical cross-sections are made every 50 mm; (b) example cross-section at x = 50 mm. The erodible bed consists of alternating layers of colored and non-colored sand, which are used to reconstruct basal scour depth at the cross-sections; (c) basal scour depth is reconstructed using image analysis; (d) a basal scour depth map is reconstructed by interpolation of the measured scour depth values at the cross-sections.

the debris-flow tail (cf. De Haas *et al.*, 2015a). In most experiments the initially eroded surface was buried by subsequent deposition nevertheless, and therefore scour depth needed to be reconstructed from vertical sections (Figure 3). Debris flows were released from a mixing tank connected to the upstream end of the flume channel. Sediment and water were agitated in the mixing tank for ∼20 s and agitation stopped simultaneously to gate opening. The gate opened electromagnetically by swinging upwards, which enabled rapid release of well-mixed debris.

Flow velocity and flow depth were visually inferred from movies shot with a Canon Powershot A650 IS (cf. De Haas *et al.*, 2015a). Average frontal flow velocity in the lower 0.6 m of the fixed bed (1.4–2.0 m downstream of the start of the channel) was used as representative velocity in this study. Flow depth was measured at the fixed to erodible bed transition, by reading the flow depth at time x since opening of the gate from the tape measure from the movie shot with the Canon Powershot camera. This ignores potential variations in cross-sectional flow depth, but based on movies of the flow in the confined experimental channel (see supplementary movies S1–S8, provided as supporting information) we estimate the potential variations in cross-sectional flow depth to be within 10% of the total flow depth. As such, we estimate that the

accuracy associated with the flow depth measurements to be <2–3 mm.

The erodible bed consisted of alternating layers of colored and non-colored sand. The non-colored sand had a maximum grain size of 1.7 mm (Figure 2). The colored sand consisted of quartz sand ranging between 2 and 5 mm in diameter (granucol); blue, green, yellow and red colored sand was used. Basal scour was measured as follows (Figure 3). A vertical cross-section was made every 5 cm along the erodible bed (Figure 3a). A photograph was made of each cross-section from which the scour depth was reconstructed, after correction for lens distortion (Figure 3b, c). Pixel size was determined from a 10 cm ruler that was placed in each photograph. Scour depth was determined as the depth up to where colored sand layers were removed. A continuous scour depth map was constructed by interpolating the measured scour depth values at the cross-sections, using triangulation-based cubic interpolation (Figure 3d).

In all experiments the erodible bed consisted of dry sediments. To minimize variations in compaction of the bed sediment, the following procedure was employed to create the erodible bed. First, the bed was formed by depositing the different colored and non-colored sand layer by layer using a sieve (resulting in near-random loose packing), and then the bed was uniformly compacted by tapping with a concrete

trowel (resulting in near-random close packing). As the erodible bed consisted of the same sediment for each experimental run and approached close packing porosity values (which is a fixed value (e.g. Song *et al.*, 2008)), we estimate that initial bed sediment porosity was similar within a few percent. Accordingly we estimate that variations in initial bed sediment porosity and compaction only had a limited effect on the measured amounts of erosion.

Data reduction

Mean and maximum erosion were used to describe the amount of basal scour. Mean erosion is defined as the mean erosion depth, averaged over the entire erodible bed, and maximum erosion is defined as the maximum scour depth observed on the erodible bed.

To quantify the spatial scour pattern, the scour asymmetry ratio (A) is introduced. Scour asymmetry is defined as the ratio between the maximum scour depth in the upper ($x = 0$–$0.5L$) and lower half ($x = 0.5$–L) of the bed:

$$A = \frac{\max \text{scour}_{x=0-0.5L}}{\max \text{scour}_{x=0.5L-L}} \quad (1)$$

Asymmetry values above 1 indicate more erosion in the upper half of the bed, whereas values below 1 imply the opposite.

Sediment erosion by debris flows may occur when sediment is mobilized by basal shear forces (e.g. Takahashi, 1981; Hungr *et al.*, 2005), or it may be related to grain-collisional stresses arising from the shear of the granular material (e.g., Stock and Dietrich, 2006; Hsu *et al.*, 2008; Reid *et al.*, 2011). The basal shear force exerted on the bed by the flowing mixture of debris is estimated by its shear stress (τ in Pa):

$$\tau = \rho g H \sin(S) \quad (2)$$

where ρ is the density of the flow (kg m^{-3}), g is the gravitational acceleration (m s^{-2}), H is flow depth (m) and S is the channel bed slope. We approximate the density of the flow as its bulk density in a perfectly mixed debris flow, and use the maximum flow depth as input for flow depth. Note that this introduces small errors, as flow depth is not constant over time and neither is the flow density, as the flow front generally develops a relatively high solids fraction.

The collisional stress σ_{gc} (Pa) within the experimental debris flows is approximated as (cf. Stock and Dietrich, 2006; Hsu *et al.*, 2008; Yohannes *et al.*, 2012):

$$\sigma_{gc} = v_s \rho_s D^2 \gamma^2 \quad (3)$$

where v_s is the volumetric solids fraction (–), ρ_s is the solid particle density (kg m^{-3}), and D is the characteristic particle diameter (m), which is approximated by the median particle size of the entire debris flow here for lack of quantitative particle-size segregation data. The shear rate γ (s^{-1}) is defined as (cf. Savage and Hutter, 1989; Iverson, 1997):

$$\gamma = \frac{u}{H} \quad (4)$$

where u is flow velocity (m s^{-1}). This approximation of shear rate assumes a linear vertical velocity distribution. In reality, the vertical velocity distribution generally deviates from linear in debris flows (Kaitna *et al.*, 2014), but due to a lack of data on the vertical velocity distribution of the experimental debris flows presented here we estimate shear rate as given in Equation (4).

Results

Debris-flow characteristics

The experimental debris flows came down the channel in one major and a few minor surges (Figure 4; movies S1–S8). Flow depth increased rapidly at the flow front and decreased more gradually after the flow front had passed. Flow depths were highest at the flow front and decreased towards the debris-flow tail. Multiple small surge fronts were present in the debris-flow tail, as shown by the multiple small peaks in flow depth in Figure 4. All debris flows had a frictional flow regime, except for the clay++ flows, which had a viscous flow regime because of their high clay fraction (see Figure 6 and Section 3.2 in De Haas *et al.*, 2015a, for details on the flow regime of these experimental debris flows).

A coarse-grained flow front was observed to develop in all experimental debris flows that had a frictional flow regime. Flow velocity in the coarse-grained flow front was lower than the velocity of the finer-grained, more dilute and liquefied material behind the flow front (i.e. flow body). As a result, the flow body continuously shouldered the flow front forwards and aside. This did not generally result in the deposition of lateral levees as flows were typically confined by the channel walls.

Flow depth increased with flow velocity (Figure 5a). For a similar velocity, the clay-rich experimental debris flows have a relatively low flow depth, while large flow depths are present in the gravel+ and water+ and water++ debris flows. Despite this general trend, variability is high; for example, some clay-rich debris flows had higher flow depths than gravel-rich debris flows for similar velocity. In general, flow velocity increases linearly with channel slope (Figure 5b). For a similar channel slope, flow velocity increases with decreasing grain size and increasing water fraction. Nevertheless, the flow velocity in the clay+ debris flows exceeds the flow velocity in the clay++ debris flows on a similar slope, which is caused by the viscous flow regime in the latter flows. The relatively low flow velocity of the coarser-grained debris flows is probably caused by the increasingly large accumulation of coarse particles at the flow front, which forms a mobile dam that increases frontal friction and thereby decreases flow velocity. Flow velocity initially increases with water fraction from fractions of 0.40 to 0.54, after which the increase appears to stagnate as the flow velocities of the water+ and water++ debris flows are approximately similar. Flow depth increases with slope for most debris-flow types, but there is considerable scatter in the trends (Figure 5c). The flow depth of some of the water-rich debris flows (water+ and water++) sharply increases
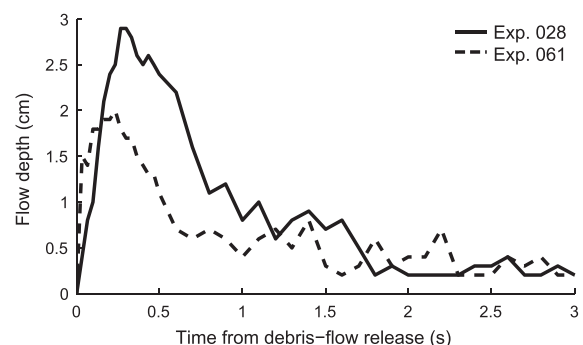

Figure 4. Characteristic development of flow depth over time; examples from experiments 028 (water+) and 061 (gravel++). Maximum flow depth is located at the flow front and small surges occur in the debris-flow tail.
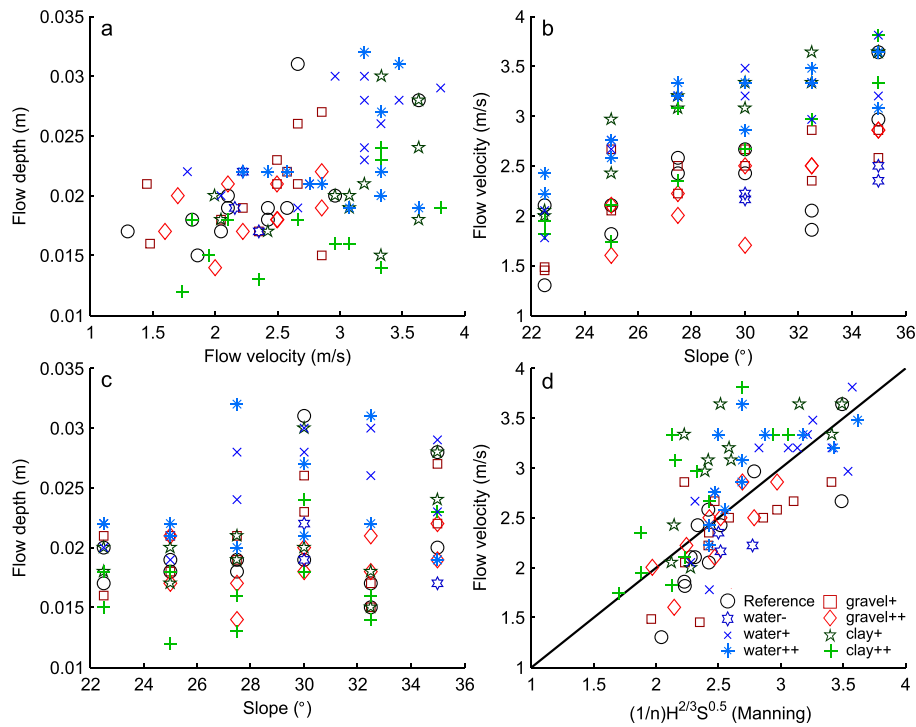
Figure 5. Flow characteristics: (a) relation between flow velocity and flow depth; (b) relation between channel slope and flow velocity; (c) relation between channel slope and flow depth; (d) relation between Manning's equation and flow velocity. Manning's equation is given as $(1/n)H^{2/3}S^{0.5}$, where n is Manning's roughness coefficient. Here we use $n = 0.02$, which results in the best fit between Manning's equation outcome and measured flow velocity ($R^2 = 0.43$).

for gradients larger than 27.5°. The flow depth appears to be relatively low for a channel gradient of 32.5°, compared to 30° and 35° gradients. Flow velocity correlates well with Manning's equation ($(1/n)H^{2/3}S^{0.5}$, where n is Manning's roughness coefficient) (Figure 5d). A roughness coefficient of 0.02 results in the best correlation between measured flow velocity and the outcomes of Manning's equation. However, in general, Manning's equation with a roughness coefficient of 0.02 underpredicts the flow velocity of clay-rich debris flows and tends to overpredict the flow velocity of the gravel-rich debris flows. A Manning's roughness coefficient of 0.02 is at the lower boundary of roughness coefficients found in natural debris flows (Rickenmann, 1999). Rickenmann (1999) found that a Manning's roughness coefficient of 0.1 leads to the best correlation between measured and predicted flow velocity in a large dataset of natural debris flows. They further show that Manning's roughness coefficients decrease with decreasing peak discharge. Nevertheless, the higher flow resistance in natural debris flows compared to our experimental debris flows probably predominantly results from the larger bed roughness in natural streams, caused by, for example, the presence of bed forms, step-pools and large boulders in the channel.

Flow velocity decreased over the erodible bed by 20% on average, but the deceleration can be up to 50%. In two out of the 86 experimental debris flows a slight increase in flow velocity was observed. There are no large differences in velocity decrease between debris flows with different compositions. In general, we observed a relatively large decrease in frontal flow velocity at the upstream part of the erodible bed, after which a second flow surge increased the flow velocity over the erodible bed again. When the debris flows move over the erodible bed, the pores in the flow and the bed become connected and pore pressure transmission occurs (Iverson et al., 2011). This leads to a decrease in pore pressure in the debris flows as a result of the dry bed and consequently a decrease

in velocity (Iverson et al., 2011; Reid et al., 2011). Moreover, bed entrainment adds flow mass with zero velocity, which also leads to a decrease in flow velocity (Iverson et al., 2011).

Erosional mechanisms

We inferred bed entrainment mechanisms from the spatial patterns of entrained bed material in cross-sections of the debris-flow deposits (Figure 6). The experimental debris flows were observed to progressively erode the bed by (i) incorporating the bed sediments grain by grain and (ii) en masse failure of parts of the bed.

Colored sediment was well incorporated in some debris flows, but concentrations of colored sediments in others indicate entrainment but no complete diffusion of sediment. En masse failure of parts of the bed becomes evident from the downstream displacement of colored layers of bed sediment that are still largely intact. Examples are shown in Figure 6e and f, where an intact layer of green and blue sediment, respectively, that was eroded upstream is located above the original colored sand layer in its original configuration. En masse entrainment occurs in the form of localized failures of parts of the bed rather than large failures over substantial portions of the bed. Evidence for grain-by-grain entrainment comes from cross-sections wherein colored sediment concentration gradually decreases above a colored sediment layer (Figure 6a). Although we cannot exclude that the colored sediment might have been incorporated en masse and subsequently diffused, the uniform lateral distribution and the upward decrease in colored particles strongly suggest grain-by-grain incorporation as the most likely entrainment mechanism (Figure 6a).

The Coulomb stability model (e.g. Takahashi, 1978) implies that channel beds become more prone to en masse bed failure with increasing channel bed slope (e.g. Prancevic et al., 2014),
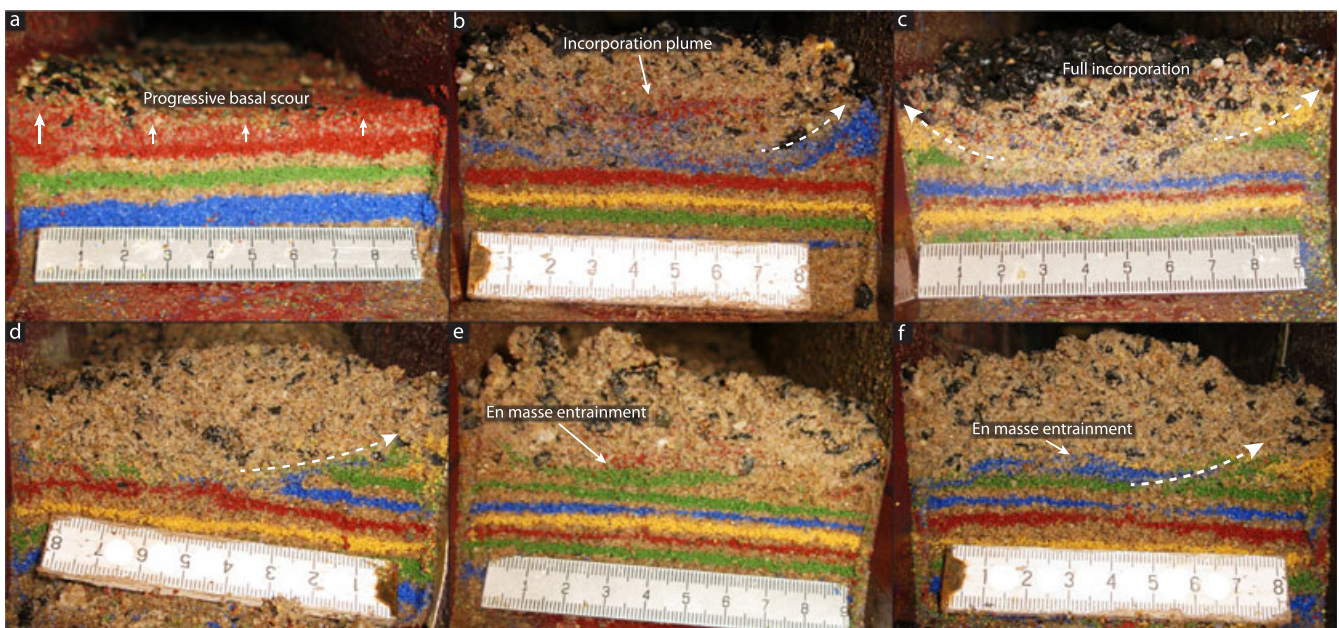
Figure 6. Erosion mechanisms. The bed sediment was scoured by progressively entraining bed sediments grain by grain and by en masse failure of parts of the bed. Much erosion probably occurred at the flow front, as the spatial patterns of the colored sediment reflect the flow patterns at the debris-flow front (see dashed lines) (e.g. Johnson *et al.*, 2012): (a) Progressive grain by grain scour of the red sediment layer (water++, experiment 029, $x = 400$ mm); (b) concentration of red and blue sediment (eroded upstream from the blue and red layers that are still largely intact below in this cross-section) in the middle of the debris flows, and sidewards displacement of the blue sediment layer following the flow patterns at the debris-flow front (gravel+, experiment 044, $x = 350$ mm); (c) full incorporation of well-mixed colored sand in the debris flow (gravel++, experiment 054, $x = 450$ mm); (d) sidewards displacement of the green sediment layer following the flow patterns at the debris-flow front (water−, experiment 016, $x = 300$ mm); (e) en masse entrainment of the green sediment layer (the upper green layer was eroded upstream from the green layer below in this cross-section) (reference, experiment 005, $x = 450$ mm); (f) en masse entrainment of the blue sediment layer and sidewards displacement of the green sediment layer following the flow patterns at the debris-flow front (water−, experiment 016, $x = 400$ mm). x denotes location of the cross-section in distance downstream of the start of the erodible bed (Figure 3).

but we could not test this as sediment was generally fully evacuated from the erodible bed at relatively high channel slopes, so that cross-sections did not reveal any information on upstream eroded material at relatively steep slopes.

The spatial patterns of colored sediment in the cross-sections of the debris flows suggest that significant entrainment occurs at the flow front (Figure 6b, c, d, f; dashed white line). In many cross-sections sand is removed from the bed in the middle of the flow and transported towards the sides. This reflects the flow patterns at the flow front of debris flows (e.g. Johnson *et al.*, 2012), where material is shouldered sidewards and is deposited in lateral levees.

Spatial scour patterns

The spatial scour patterns are largely unaffected by channel slope. Erosion asymmetry is largely similar for the different debris-flow types over a range of slopes from 22.5° to 35° (Figure 7; dataset S2). Therefore, we analyze the effects of debris-flow composition on spatial scour patterns by averaging the spatial scour depth for all runs over the full range of slopes per debris-flow type (Figure 8).

The spatial pattern of scour depth varies between different types of debris flows (Figures 8 and 9), but variability can also be large between debris flows of similar composition. In 66% of the experimental debris flows maximum scour depth occurred in the upstream half of the erodible bed, and in 83% of these experiments maximum scour depth occurred in the first 10 cm of the erodible bed. The peak erosion depth for most debris flows is located slightly downstream of the fixed to erodible bed transition. Behind this peak the scour depth is generally low, and scour depth gradually increases further

downstream (Figures 8 and 9). The processes leading to this spatial erosion pattern are unknown. It may be ascribed to the flow behavior over the erodible bed, where flow velocity initially drops when entering the erodible bed, after which a second surge increases flow velocity again further downstream (movies S1–S8). Alternatively, the scour hole might deflect the flow against gravity, leaving a reach with less erosion followed again by a reach of more erosion in the lower part of the erodible section, probably due to a bed-normal flow trajectory.

In general, total scour depth increases with water and gravel fraction or grain size, but decreases with clay fraction (Figures 8–10). Erosion asymmetry increases with water and gravel fraction due to an increase in the initial scour peak. The water- debris flows have their largest scour depth in the downstream half of the erodible bed, while for higher water fractions the scour depth becomes progressively larger in the upstream half of the erodible bed. The variability in scour pattern decreases with increasing water and gravel fraction, as testified by the standard deviation maps in Figures 8 and 9. The scour pattern becomes increasingly homogeneous with increasing clay fraction. The erosion asymmetry declines as the initial scour peak decreases with increasing clay fraction, and scour depths become nearly uniform in longitudinal direction for the the clay++ flows. Moreover, the variability strongly decreases with increasing clay fraction. The absence of an initial scour peak in the clay-rich debris flows might be caused by the low diffusivity of these flows, inhibiting pore-pressure diffusion between the debris flow and bed. Moreover, the viscous flow behavior of the clay-rich debris flows may inhibit substantial bed-flow interactions and thus entrainment.
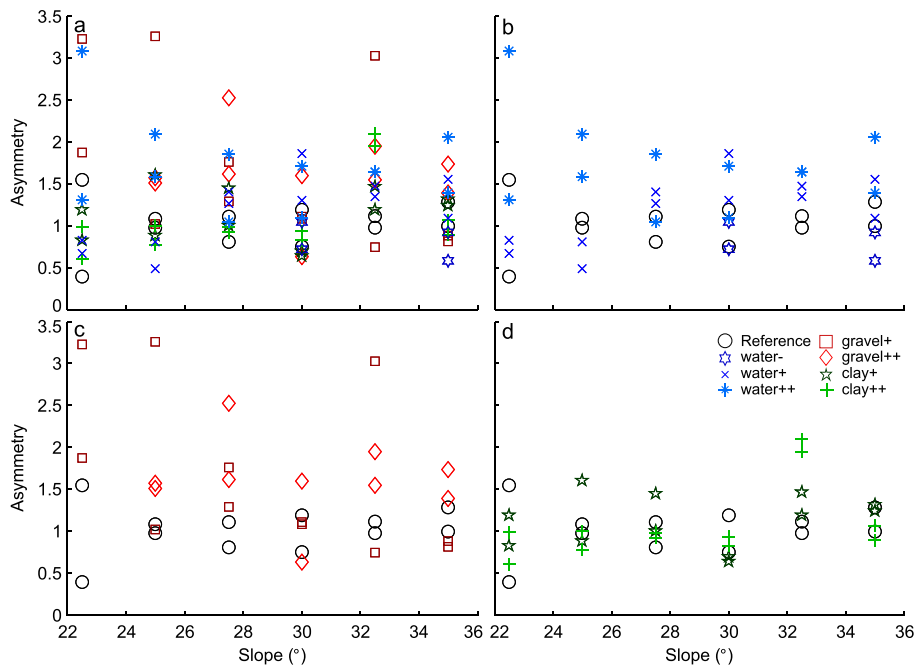
Figure 7. Relation between channel slope and basal scour depth asymmetry. Basal scour depth asymmetry is independent of channel slope for all debris-flow types: (a) all experiments; (b) water fraction series; (c) gravel fraction series; (d) clay fraction series.
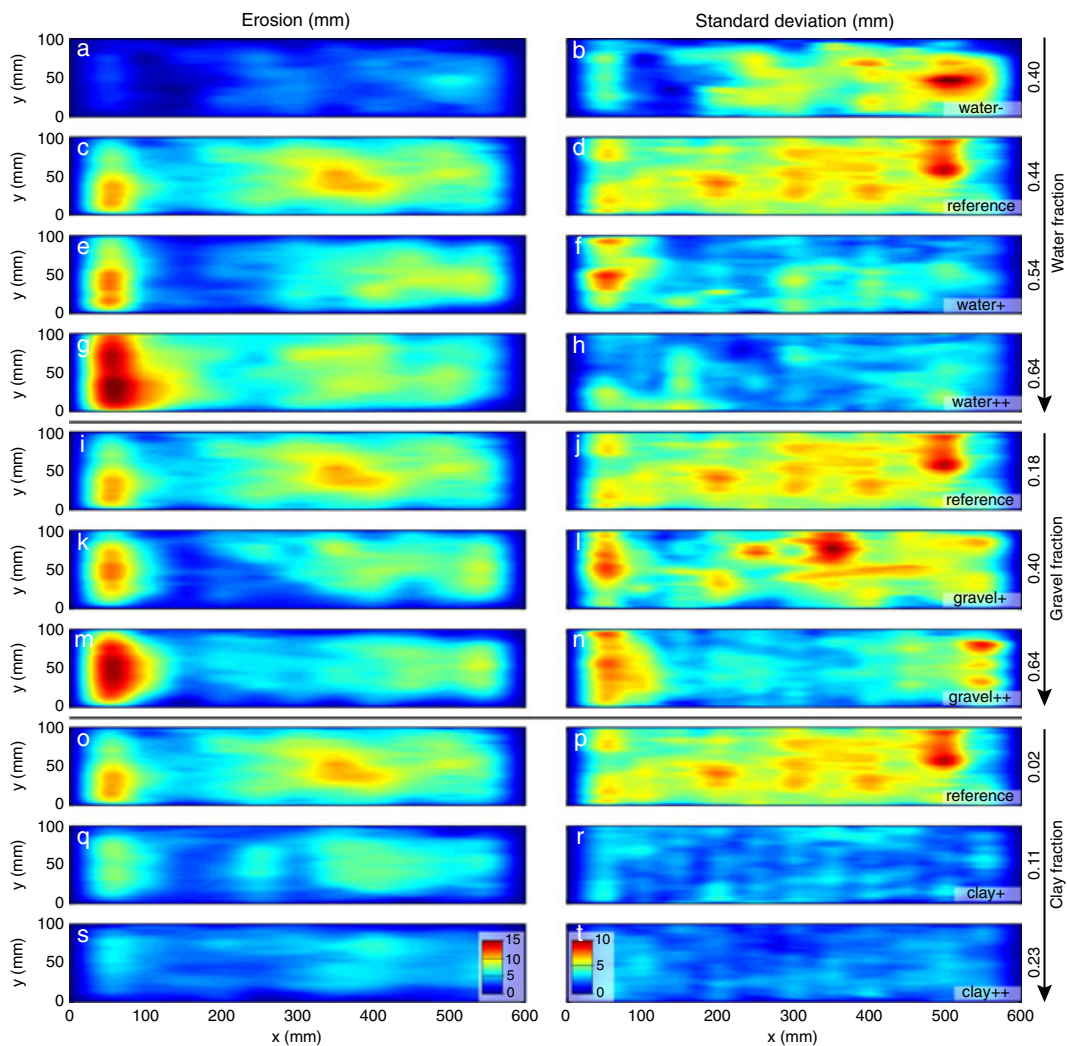

Figure 8. Basal scour depth averaged per debris-flow type and associated standard deviation. Flow from left to right. The number of averaged debris-flow scour patterns n is 12 for all images except for the water− series, and debris flows flowed over slopes ranging from 22.5° to 35°. For the water− images $n = 4$, and the averaged map only includes flows on slopes of 30° and 35°. Slope does not significantly influence spatial patterns of basal scour depth (Figure 7). See dataset S2 for basal scour maps of all the individual experimental debris flows.
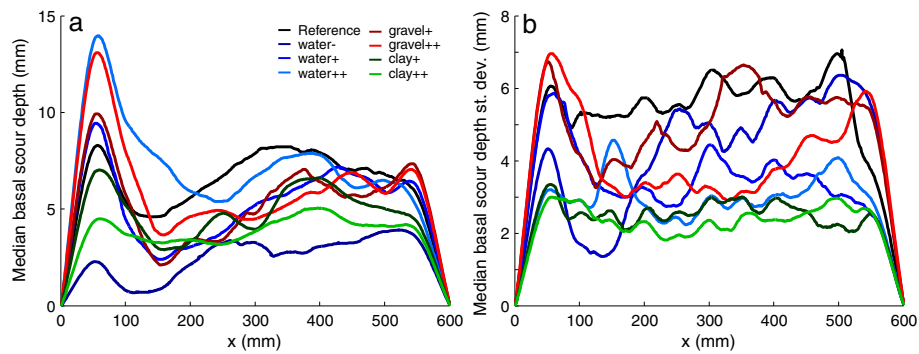
Figure 9. Median basal scour depth (a) and associated standard deviation (b) per *x* coordinate along the erodible bed per debris-flow type. Values are based on the maps in Figure 8. Flow from left to right. See dataset S2 for the median basal scour depth per *x* coordinate of all the individual experimental debris flows.
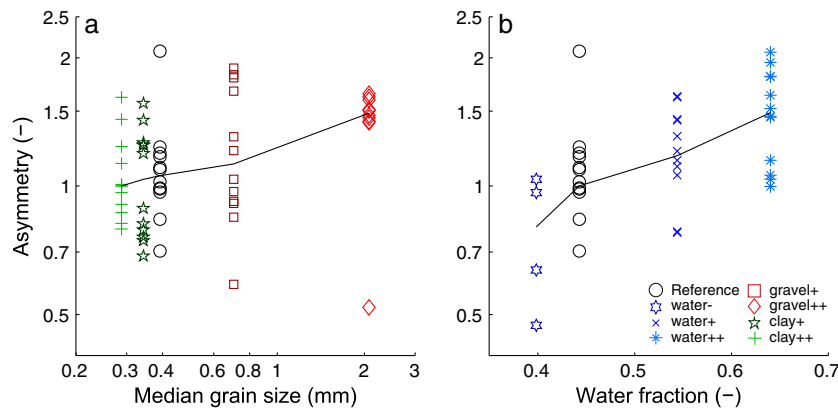

Figure 10. Relation between basal scour depth asymmetry and median grain size (a) and volumetric water fraction (b). Solid line connects mean asymmetry per median grain size and water fraction value.

Factors controlling erosion and effects of debris-flow composition

Here we evaluate the factors controlling erosion at a fixed to erodible bed transition and the effects of debris-flow composition thereon. The relation between mean and maximum basal scour depth and channel slope, flow velocity, flow depth, discharge, basal shear stress and grain collisional stress is statistically evaluated using a linear regression analysis (Figures 11 and 12; Table II). The available data suggest that there is, in general, a linear relation between the various variables and basal scour, although other relations (e.g. exponential) cannot unambiguously be excluded based on the eight data points per experimental series. Note that the natural variability in debris-flow dynamics, the highly variable and stochastic nature of the bed erosion process and the small sample size per experimental series result in relatively weak statistics with relatively high *p*-values. No statistical analysis has been performed for the water- series, as it only includes 3–4 data points.

In general, the amount of basal scour increases with increasing channel slope, flow velocity, flow depth, discharge and shear stress, whereas there is a very poor to no relation between basal scour and grain collisional stress calculated with Equation 3 (Figures 11 and 12; Table II). Below, the relation of scour depth to the above-described variables is discussed in detail, together with the effects of debris-flow composition.

Basal scour increases with channel slope for all debris-flow compositions except for gravel++ (Figures 11a and 12a). There is considerable scatter on the relationships; for mean scour

depth the goodness-of-fit R^2 ranges between 0.17 and 0.45 and corresponding *p*-values range between 0.02 and 0.19. The reference and clay-rich debris flows exhibit the strongest relations with mean erosion $R^2 > 0.33$ and *p*-values < 0.05 (Table II). The relations with maximum erosion are less strong, exhibiting lower values of R^2 and higher *p*-values (Table II). The highest values of mean and maximum erosion are found at a channel slope of 30° for most debris-flow types. Above this slope the amount of erosion becomes less, decreasing strongly at a channel slope of 32.5°, and slightly increasing again towards a channel slope of 35°. This trend corresponds to the observed relatively low water depth at a slope of 32.5° (Figure 5c). The reference and gravel-rich (gravel+ and gravel++) debris flows have the highest increase in scour at a 30° slope; their mean and maximum scour depth at a 30° channel slope exceed the scour depth at a 27.5° slope up to a factor 5 (Figures 11m and 12m). For the water-rich and clay-rich debris flows, the difference is below a factor of 2 (Figures 11g, s and 12g, s). The water+ composition has its maximum erosion at 30°, but the water++ already has its maximum erosion at 27.5° (Figures 11g and 12g). In contrast to all other debris-flow types, the mean and maximum scour depth of the gravel++ debris flows are unrelated to channel slope ($R^2 = 0.01$, $p = 0.83$ for mean erosion; $R^2 = 0.004$, $p = 0.86$ for maximum erosion): mean and maximum scour depth remain nearly constant over 25–35° channel slopes (Figures 11m and 12m; Table II). For channel slopes <30° mean and maximum scour depth increase with increasing water fraction, whereas the mean and maximum scour depths are roughly similar for channel slopes of 30° and higher (Figures 11g and 12g). Mean scour depth is roughly
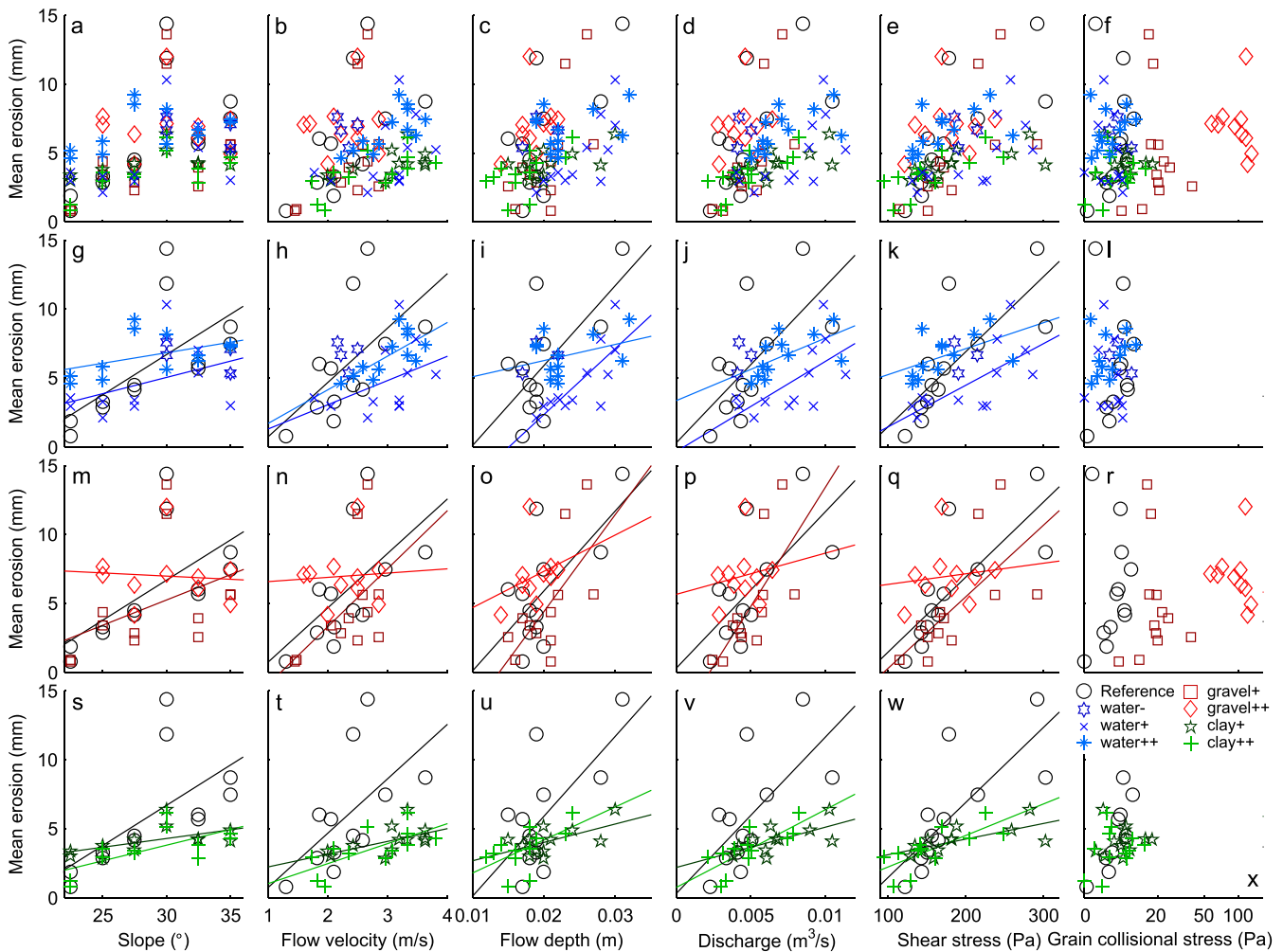
Figure 11. Relation between mean erosion and channel slope, flow velocity, flow depth, discharge, shear stress and grain collisional stress. The upper row shows all experiments; the rows below show the data for the water fraction, gravel fraction and clay fraction series, respectively. Solid lines are the linear regression lines per data series (see Table II for regression coefficients and corresponding R^2 and *p*-value. No regression lines are plotted for grain collisional stress because of the absence of a correlation, and for the water− series as these comprise only 3–4 measurement points).

similar for the reference, clay+ and clay++ debris flows for slopes <30°, whereas the scour depth is higher in the reference debris flows for slopes of 30° and higher (Figure 11s). Maximum scour depth decreases with increasing clay content on all slopes (Figure 12s).

Mean and maximum basal scour depth increase with flow velocity, flow depth, discharge and shear stress (Figures 11b–e and 12b–e). However, the mean and maximum erosion caused by the gravel++ debris flows is unrelated to these variables. The strongest correlations are found between scour depth and (i) basal shear stress and (ii) discharge; for mean erosion R^2 values are roughly in the range 0.4–0.6 and *p*-values are mostly below 0.05 (Table II). The relations with maximum erosion have lower values of R^2 and higher *p*-values and these relations are therefore less strong than the relations with mean erosion (Table II). In general, for a similar flow velocity, flow depth, discharge and shear stress, an increase in volumetric water fraction from 0.44 (reference) to 0.54 (water+) leads to decreasing mean and maximum basal scour, whereas for a water fraction of 0.64 (water++) basal scour increases again (Figures 11h–k and 12h–k). This suggests that the experimental debris flows were least erosive around a water fraction of 0.54. Mean and maximum scour depth increase roughly similarly with flow velocity, flow depth, discharge and shear stress between the reference (gravel fraction 0.18) and gravel+

(gravel fraction 0.40) debris flows (Figures 11n–q and 12n–q). However, the amount of basal scour caused by the gravel++ debris flows (gravel fraction 0.64) is roughly uniform on the full range of flow velocity, flow depth, discharge and shear stress. As a result, these flows cause relatively much erosion for relatively low values of flow velocity, flow depth, discharge and shear stress, and relatively little erosion for relatively high values of these variables. There is thus a sharp transition at a gravel fraction between 0.4 and 0.64, at which the erosive behavior of debris flows changes and becomes insensitive to flow properties such as velocity, depth, discharge and shear stress. Mean and maximum erosion decrease with increasing clay content at similar velocity, flow depth, discharge and shear stress from the reference (clay fraction 0.02) to the clay+ (clay fraction 0.11) and clay++ (clay fraction 0.23) debris flows (Figures 11t–w and 12t–w). However, the mean scour depth is approximately similar for the clay+ and clay++ debris flows (Figure 11t–w), whereas the maximum scour depth is smaller for the clay++ debris flows compared to the clay+ flows (Figure 12t–w).

Mean and maximum erosion are unrelated to grain collisional stress as expressed by Equation (3) (Figures 11f, i, r, x and 12f, i, r, x; Table II). The goodness-of-fit for the mean and maximum erosion values is typically below 0.1 and *p*-values are typically larger than 0.3.
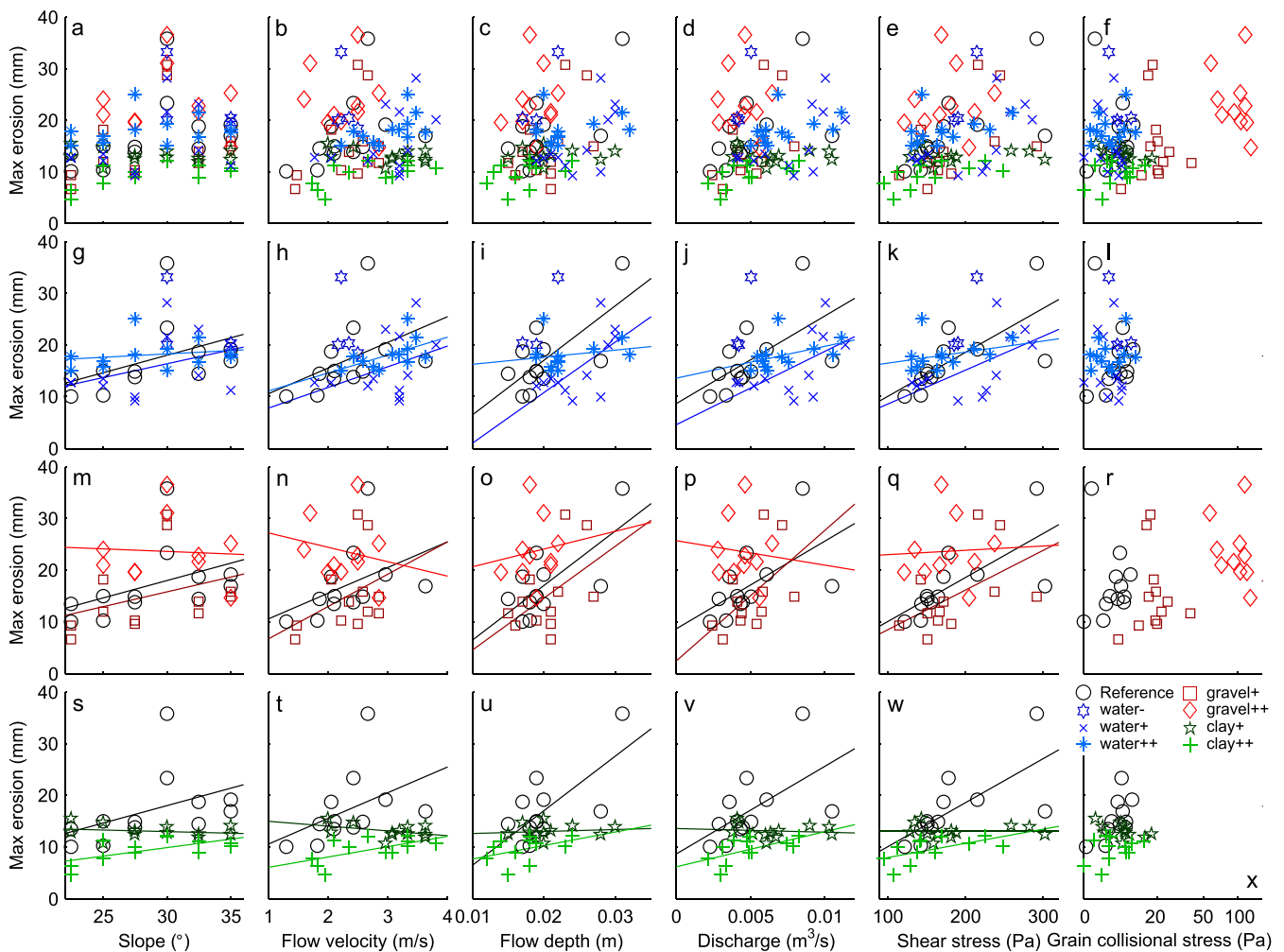
Figure 12. Relation between maximum erosion and channel slope, flow velocity, flow depth, discharge, shear stress and grain collisional stress. The upper row shows all experiments; the rows below show the data for the water fraction, gravel fraction and clay fraction series, respectively. Solid lines are the linear regression lines per data series (see Table II for regression coefficients and corresponding R^2 and *p*-value. No regression lines are plotted for grain collisional stress because of the absence of a correlation, and for the water− series as these comprise only 3–4 measurement points).

In summary, for similar topographic and flow conditions scour depth depends on composition in our experiments. Clay-rich debris flows are less erosive than gravel-rich or water-rich debris flows. In general, mean and maximum scour depth become larger with increasing water fraction and decrease with increasing clay fraction. An increase in gravel fraction results in a change in response to topographic forcings and flow conditions: mean and maximum scour depth increase with increasing slope, flow depth, flow velocity, discharge and shear stress for debris flows with gravel fractions up to 0.40, while at a gravel fraction of 0.64 the basal scour depth is unrelated to these topographic forcings and flow conditions. Scour depth was found to correlate best with basal shear stress and discharge.

Discussion

In this section we discuss the controls on debris-flow scour and erosion and the effects of debris-flow composition thereon, thresholds for incipient bed scour and spatial scour patterns. We end the discussion with a brief consideration on the translation of the experimental results presented here to natural debris-flow systems. The experiments presented here mainly simulated erosion at the transition from fixed to erodible bed. However, below we mainly compare our experimental findings to observations of erosion in natural debris-flow torrents with more spatially continuous erodible beds due to a lack of observations on scour and erosion by debris flows downstream of a fixed to erodible bed transition. Although there will be differences in erosion patterns between these two bed configurations, the hydrodynamic and topographic controls on the erodibility of debris flows will be largely similar.

Effects of debris-flow composition on bed scour and erosion

In our experimental debris flows basal scour increases with basal shear stress, flow discharge, flow velocity, flow depth and channel slope (Figures 11 and 12). This is in good agreement with observations from natural debris flows (e.g. Rickenmann *et al.*, 2003; Chen *et al.*, 2005; Conway *et al.*, 2010; Schürch *et al.*, 2011; Berger *et al.*, 2011; Theule *et al.*, 2015). In general, basal scour increased with increasing debris-flow grain size, in agreement with the experimental findings of Egashira *et al.* (2001) showing that erosion increases as the ratio between the debris-flow grain size and the bed grain size becomes larger. We experimentally show that the experimental debris flows were least erosive around

Table II. Linear regression statistics for the data presented in Figures 11 and 12

Variable	Debris flow	Mean erosion statistics				Max erosion statistics			
		a	b	R^2	p	a	b	R^2	p
slope	Reference	0.58	−10.78	0.41	0.03	0.67	−2.11	0.18	0.16
	water+	0.24	−2.04	0.18	0.17	0.54	0.09	0.16	0.19
	water++	0.15	2.19	0.21	0.13	0.13	14.35	0.04	0.52
	gravel+	0.36	−5.71	0.17	0.19	0.57	−1.34	0.12	0.28
	gravel++	−0.04	8.31	0.01	0.83	−0.1	26.72	0	0.86
	clay+	0.13	0.44	0.33	0.05	−0.06	14.86	0.05	0.51
	clay++	0.23	−2.98	0.45	0.02	0.33	0.08	0.4	0.03
Flow velocity	Reference	3.94	−3.22	0.34	0.04	4.95	5.6	0.19	0.16
	water+	1.75	−0.45	0.17	0.19	3.99	3.83	0.15	0.22
	water++	2.43	−0.71	0.52	0.01	3.45	7.66	0.3	0.07
	gravel+	4.2	−5.08	0.25	0.1	6.26	0.41	0.16	0.2
	gravel++	0.31	6.25	0	0.86	−2.76	29.92	0.04	0.59
	clay+	0.93	1.32	0.29	0.07	−0.96	15.97	0.18	0.17
	clay++	1.45	−0.42	0.46	0.02	2.01	4.05	0.37	0.03
Flow depth	Reference	580.46	−5.69	0.44	0.02	1056.41	−4.08	0.5	0.01
	water+	479.73	−7.24	0.6	0	980.48	−8.84	0.43	0.02
	water++	116.93	3.93	0.12	0.28	134.6	14.95	0.04	0.51
	gravel+	704.19	−9.65	0.44	0.02	1006.09	−5.51	0.25	0.1
	gravel++	263.56	2.04	0.09	0.39	346.21	17.13	0.02	0.71
	clay+	132.65	1.36	0.35	0.04	38.14	12.26	0.02	0.69
	clay++	239.21	−0.6	0.34	0.05	262.06	5	0.17	0.18
Discharge	Reference	1134.57	0.29	0.44	0.02	1700.14	8.64	0.34	0.05
	water+	651.82	−0.33	0.4	0.03	1421.57	4.59	0.33	0.05
	water++	453.86	3.34	0.37	0.04	615.1	13.61	0.19	0.16
	gravel+	1727.38	−3.9	0.49	0.01	2524.84	2.42	0.29	0.07
	gravel++	299.79	5.64	0.03	0.64	−475.63	25.71	0.01	0.8
	clay+	290.94	2.2	0.44	0.02	−72.17	13.53	0.02	0.7
	clay++	559.73	0.76	0.56	0.01	673.49	6.19	0.35	0.04
Shear stress	Reference	0.05	−4.03	0.61	0	0.09	1.55	0.51	0.01
	water+	0.03	−1.58	0.46	0.02	0.07	1.92	0.37	0.04
	water++	0.02	3.38	0.27	0.09	0.02	14.37	0.1	0.32
	gravel+	0.05	−4.9	0.44	0.02	0.08	0.78	0.27	0.08
	gravel++	0.01	5.6	0.02	0.71	0.01	22.08	0	0.89
	clay+	0.01	1.97	0.45	0.02	0	13.03	0	0.99
	clay++	0.02	−0.07	0.53	0.01	0.03	5.16	0.33	0.05
Grain collisional	Reference	0	3.66	0.04	0.55	0	17.85	0	0.95
	water+	−0.94	7.29	0.09	0.35	−1.57	19.91	0.04	0.52
	water++	0.4	5.54	0.1	0.31	0.57	16.5	0.06	0.44
	gravel+	−0.09	5.73	0.02	0.69	−0.13	16.5	0.01	0.76
	gravel++	−0.01	8.11	0.03	0.61	−0.06	29.08	0.09	0.4
	clay+	0.01	4.09	0	0.96	−0.29	14.23	0.19	0.15
	clay++	0.19	2.89	0.04	0.52	0.45	8	0.1	0.31

Note: The coefficients a and b correspond to the regression line $y = ax + b$. R^2 denotes the goodness-of-fit of the regression line. A p-value < 0.05 denotes that there is a significant correlation between mean erosion and a given variable.

a water fraction of 0.54, and that mean scour depth increases for lower and higher water fractions relative to this value. This trend contradicts the findings of Egashira *et al.* (2001), Hungr *et al.* (2005) and Fagents and Baloga (2006) that suggest that erosion increases with water fraction, and Rickenmann *et al.* (2003), who experimentally found that the erosion rate initially increases with volumetric sediment concentration, whereas the erosion rate decreases above a volumetric sediment concentration of 0.4. Grain collisional stresses did not exert a large control on bed scour in our experiments, in contrast to observations from bedrock erosion by debris flow (e.g. Stock and Dietrich, 2006; Hsu *et al.*, 2008, 2014; Yohannes *et al.*, 2012).

The correlation between bed scour and basal shear stress and absence of a relation between bed scour and grain collisional stress (Figures 11 and 12) is probably caused by the small influence of grain collisional stress relative to basal shear stress in the experimental debris flows. In most experiments grain collisional stresses account for <5% of the total stress (basal shear stress and grain collisional stress combined); only for the gravel++ debris flows does grain collisional stress have a substantial contribution to the total stress with (30–50%). Figure 13 illustrates the influence of grain collisional stress (Equation (3)) relative to total stress (basal shear stress, Equation (2), and grain collisional stress combined) for a range of characteristic debris-flow grain sizes and debris flows
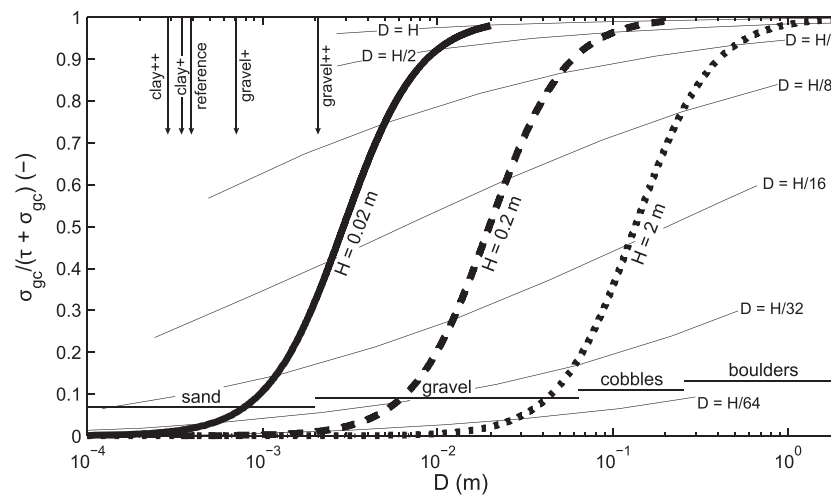
Figure 13. Influence of grain collisional stress (σ_{gc}, Equation (3)) relative to total stress (basal shear stress (τ, Equation (2)) and grain collisional stress combined) for a range of characteristic debris-flow grain sizes. The thick lines represent flow depths of 0.02, 0.2 and 2 m; the thin lines illustrate the ratio between characteristic grain size and flow depth. The arrows at the top left denote the characteristic grain size of the different types of experimental debris flows studied here (corresponding to the line for $H = 0.02$ m). Flow velocity corresponding to the various flow depths was calculated using Manning's equation, with a roughness coefficient n of 0.02 (cf. Figure 5d). The following constants were used for the calculation shown here: $\rho = 1920$ kg m^{-3}, $\rho_s = 2650$ kg m^{-3}, $v_s = 0.5$, $g = 9.81$ m s^2, S is 30°.

of various flow depth in an idealized model. In this model flow velocity corresponding to the various flow depths was calculated using Manning's equation, with a roughness coefficient n of 0.02 (cf. Figure 5d). The model is based on our experimental setup and the following constants were used as model input: $\rho = 1920$ kg m^{-3}, $\rho_s = 2650$ kg m^{-3}, $v_s = 0.5$, $g = 9.81$ m s^2, S is 30°. The model shows that in debris flows with a depth of 0.02 m, similar to the flow depth in our experiments, grain collisional stresses may have a substantial effect on basal scour when the characteristic grain size exceeds 1/16–1/8 of the flow depth. This corresponds well to the experimental observation that basal scour is strongly dependent on basal shear stress in the reference, water−, water+, water++, clay+, clay++ and gravel+ debris flows as the relative effect of grain collisional stress is very small in these flows. Moreover, the deviant behavior of the gravel++ debris flows, being unrelated to basal shear stress, might be explained by the substantial contribution of grain collisional stress in these debris flows. This model explains why erosion caused by some debris flows is mainly controlled by basal shear stress (e.g. Takahashi, 1981; Hungr et al., 2005), while erosion in other debris flows is largely controlled by grain collisional stress e.g. Stock and Dietrich, 2006; Berger et al., 2011). The model further shows that the relative effect of grain collisional stress becomes larger with increasing debris-flow size. For example, the relative influence of grain collisional stresses in a debris flow with a characteristic grain size that is 16 times smaller than the flow depth is 4 times larger in a debris flow of 2 m flow depth than in a debris flow of 0.02 m flow depth. In the former the relative influence is ∼0.45 and grain collisional stresses will therefore substantially influence bed scour, whereas for a flow depth of 0.02 m the relative influence is ∼0.13 and bed scour will mainly be influenced by basal shear stress.

Furthermore, the increase in erodibility with increasing gravel fraction in our experimental debris flows can probably be related to the increase in grain collisional stress, thereby enhancing the total stress at the bed and thus erosion. Similarly, the experimental decrease in bed scour with increasing clay fraction is probably related to (i) a decrease in grain collisional stress as well as (ii) the increasingly viscous behavior of the debris flows with increasing clay fraction (De Haas et al., 2015a).

In short, our results show that bed scour and erosion by debris flows depend strongly on debris-flow composition. The grain-size distribution relative to debris-flow size determines the relative effect of grain collisional stress and basal shear stress at the bed as well as the flow behavior (i.e. collisional, frictional or viscous). Variations in debris-flow composition might thus partly explain contradictory field observations of debris-flow erosion (e.g. Hungr 568 et al., 2005; Schürch et al., 2011). Moreover, our results suggest that the variable that best predicts erosion strongly depends on debris-flow composition. Debris flows originating from catchments yielding relatively large amounts of fines (e.g. catchments comprising shale rocks) are less likely to entrain bed sediments and grow in size than catchments that generate more larger-sized clastic sediments, and therefore have less hazardous potential. Moreover, erosion by debris flows originating from such catchments can likely be reasonably estimated by basal shear stress. In contrast, debris flows originating from catchments that are richer in coarse particles are likely to be more erosive and basal shear stress is less likely to accurately predict the amounts of erosion due to a larger influence of grain collisional stress.

Thresholds for incipient bed scour

The experimental results show that there are thresholds that need to be overcome before significant basal scour occurs (Figures 11 and 12). These thresholds vary considerably per debris-flow type, but a rough estimation of the thresholds of mean scour depth for all debris flows combined suggests that basal scour occurs above a channel slope of ∼20°, a flow velocity of ∼1 m s^{-1}, a flow depth of ∼0.01 m and a basal shear stress of ∼100 Pa. For maximum scour depth these thresholds are lower: for example, the critical slope for erosion is ∼10° when extrapolating the trend for maximum scour depth.

Such thresholds have also been identified in natural debris-flow torrents and previous experiments. Schürch et al. (2011) and Berger et al. (2011) found that substantial erosion takes place when a basal shear stress of 3–4 KPa is exceeded in the Illgraben torrent. Reported critical slopes for

debris-flow erosion in natural torrents range from ~9° for natural debris flows in two torrents in the French Alps (Theule *et al.*, 2015), 8–12° (Hungr *et al.*, 1984) or 12–15° (Guthrie *et al.*, 2010) for debris flows in British Columbia, 16° on the Kamikamihora fan in Japan (e.g., Okuda and Suwa, 1984; Takahashi, 2009) and 19° for hillslope debris flows in Iceland (Conway *et al.*, 2010). Mangeney *et al.* (2010) found that the critical slope at which erosion by granular flows on a dry erodible bed occurs is approximately half the repose angle of the erodible bed sediments. A similar critical slope was found in our experiments with wet debris flows over dry erodible beds (~20°. Pan *et al.* (2015) found that experimental debris flows with a density of 1900 kg m⁻³ and a median grain size of 0.45 mm had a critical slope for erosion on a wet bed of 11.0°. This sediment is comparable with the reference mixture of our experiments, with a density of 1919 kg m⁻³ and a median grain size of 0.39 mm, although the critical slope was much larger in our experiments, probably because of the dry erodible bed used in our experiments. There are multiple explanations for the highly variable critical slopes observed in various natural debris-flow torrents and experimental flumes. Bed erodibility increases with enhanced pore-water content in the bed (Iverson *et al.*, 2011; Reid *et al.*, 2011). Most natural debris flows are triggered during high-intensity rainfalls, which increases the water content in the bed before passage of the debris flows. Therefore, the dry bed conditions in our experiments might explain the relatively high critical slope for basal scour in our experiments. Moreover, our results show that the differences might also be explained by variations in debris-flow composition between the torrents, as well as differences in the typical flow velocities, depths, discharges and basal shear stresses and grain collisional stresses.

Spatial scour patterns

Schürch *et al.* (2011) found a high variability of erosion amounts and depths under similar-sized debris flows, as well as a high variability in spatial patterns of erosion in the Illgraben debris-flow torrent. Similarly, in our experiments the spatial patterns of scour were also highly variable between debris flows with similar composition (Figure 8) and, accordingly, measured mean and maximum erosion were highly variable (Figures 11 and 12). This most likely predominantly results from the high natural variability of flow and entrainment dynamics in debris flows. Despite the observed variability, the large-scale basal scour patterns were generally roughly similar in our experiments. The largest erosion could mostly be found at the start of the erosive bed, and scour decreased towards the end, though some extra scour peaks were almost always observed. These results suggest that many debris flows can entrain a relatively large amount of sediment directly downstream of a bedrock to colluvium transition or structure in a debris-flow torrent. This, however, depends strongly on the debris-flow composition, and enhanced erosion at the bedrock–colluvium transition will be limited in clay-rich debris flows or debris flows containing a limited water fraction.

Translation to natural systems/scaling

The generic flow behavior of our experimental debris flows was largely similar to that in natural debris flows (for a more extensive comparison to natural debris flows and scaling analysis of the current experimental debris flows, see De Haas *et al.*, 2015a). A coarse-grained flow front, followed by more dilute material, developed in our experimental debris flows. This grain-size sorting implies that the processes that govern the flow behavior and grain-size segregation of natural debris flows, such as kinematic sorting, squeeze expulsion and preferential transport of coarse particles to the flow front (e.g. Johnson *et al.*, 2012), were also present in our experimental debris flows. Additionally, the qualitative response of basal scour to debris flow forcings, including flow velocity, flow depth, flow discharge and shear stress, is similar to the response in natural systems (e.g. Rickenmann *et al.*, 2003; Chen *et al.*, 2005; Conway *et al.*, 2010; Schürch *et al.*, 2011; Berger *et al.*, 2011; Theule *et al.*, 2015). These results suggest that the trends obtained here are most likely qualitatively applicable for understanding the effects of debris-flow composition and various forcings on debris-flow erosion, as well as understanding spatial patterns and mechanisms of debris-flow erosion at a fixed to erodible bed transition. Moreover, the experimental setup presented in this study opens up the possibility to investigate erosion by debris flows in experiments under controlled conditions.

Uncertainties associated with the translation of our experimental results to natural debris-flow systems may arise as follows. Debris-flow erosion may be supply-limited in natural debris-flow torrents (Abancó and Hürlimann, 2014), potentially yielding relatively smaller amounts of bed erosion when compared to our experiments with unlimited sediment availability. On the other hand, bank collapse might enlarge erosion volumes in natural debris-flow torrents. In general, debris flows originate during periods of extensive rainfall or snowmelt and therefore channel-bed sediments are typically relatively wet, which may significantly influence the erosive behavior of the debris flows (e.g. Iverson *et al.*, 2011; Reid *et al.*, 2011). Additionally, small-scale experimental debris flows exhibit disproportionately large effects of fluid yield strength, viscous flow resistance and grain inertia, while exhibiting disproportionately small effects of pore-fluid pressure (Iverson, 1997; Iverson and Denlinger, 2001; Iverson *et al.*, 2010). This might quantitatively affect basal scour depth in our experiments compared to natural debris-flow systems, but how is unknown. In the experimental debris flows presented here, basal shear forces generally dominate over grain collisional forces. However, for a fixed flow depth to characteristic grain size ratio, the influence of grain collisional forces increases with flow depth (Figure 13). Natural debris flows for which bed erosion is substantially influenced by grain collisional stresses are thus likely to be more common. For example, in a debris flow with a flow depth of 2 m and a characteristic grain size of 0.125 m, basal shear stress and grain collisional stress will have an approximately similar influence on bed erosion.

Conclusions

We experimentally investigated the effects of debris-flow composition on bed scour by debris flows at a fixed to erodible bed transition. In particular, we investigated the erosive potential of various types of debris flows, evaluated which variables (out of channel slope, flow velocity, flow depth, discharge and shear stress and grain collisional stress) best predict basal scour depth, determined the erosion mechanisms and explored spatial scour patterns.

The experimental debris flows were observed to progressively erode the bed by (i) incorporating the bed sediments grain by grain and (ii) en masse failure of parts of the bed. Moreover, the reworking patterns in sedimentary

cross-sections of the experimental debris flows suggest that a significant amount of erosion occurred at the flow front.

The amount of basal scour increases with increasing channel slope, flow velocity, flow depth, discharge and shear stress in our experiments, whereas the basal scour is not related to grain collisional stress. The strongest correlation is between basal scour and shear stress and discharge. There are significant differences in the scour caused by different types of debris flows. In general, the clay-rich experimental debris flows are less erosive than the gravel-rich or water-rich debris flows. Mean and maximum scour depth become larger with increasing water and gravel fraction and decrease with increasing clay fraction. However, the erodibility of very coarse-grained debris flows (gravel fraction 0.64) is unrelated to topographic forcings and flow conditions: the basal scour depth of these debris flows is approximately similar on a wide range of channel slopes, flow velocities, flow depths, discharges and shear stresses. The deviant response of the coarse-grained debris flows is probably caused by the relatively large influence of grain-collisional stress to the total stress (basal shear stress and grain-collisional stress combined) at the bed in these flows (30–50%). In contrast, the relative effect of grain-collisional stress is low in the other experimental debris flows (<0.05), causing erosion to be largely controlled by basal shear stress. The increasing erosion with gravel fraction is probably related to an increase in grain collisional forces, whereas the decrease with clay fraction most likely results from a decrease in collisional forces and an increasingly viscous flow behavior.

The spatial patterns of bed scour are highly variable. Nevertheless, the large-scale scour patterns are largely similar over 22.5–35° channel slopes for debris flows of similar composition. The largest scour depth generally occurs slightly downstream of the fixed to erodible bed transition, and scour asymmetry (ratio of maximum scour depth in the upstream and downstream half of the erodible bed) is larger than 1. The bed scour asymmetry becomes larger with increasing debris-flow grain size and water fraction, while the scour depth is nearly uniform in clay-rich debris flows (asymmetry ≈ 1). The variability of the scour depth patterns becomes smaller with an increasing water, gravel (= grain size) and clay fraction in the debris flows.

References

Abancó C, Hürlimann M. 2014. Estimate of the debris-flow entrainment using field and topographical data. *Natural Hazards* **71**: 363–383.

Berger C, McArdell B, Schlunegger F. 2011. Direct measurement of channel erosion by debris flows, Illgraben, Switzerland. *Journal of Geophysical Research: Earth Surface* **116**: F01002. DOI: 10.1029/2010JF001722.

Blair TC, McPherson JG. 2009. Processes and forms of alluvial fans. In *Geomorphology of Desert Environments*, Parsons A, Abrahams A (eds), Springer: Berlin; 413–467.

Bormann NE, Julien PY. 1991. Scour downstream of grade-control structures. *Journal of Hydraulic Engineering* **117**: 579–594.

Chen H, Zhang L. 2015. EDDA 1.0: integrated simulation of debris flow erosion, deposition and property changes. *Geoscientific Model Development* **8**: 829–844.

Chen J, He Y, Wei F. 2005. Debris flow erosion and deposition in Jiangjia Gully, Yunnan, China. *Environmental Geology* **48**: 771–777.

Conway S, Decaulne A, Balme M, Murray J, Towner M. 2010. A new approach to estimating hazard posed by debris flows in the Westfjords of Iceland. *Geomorphology* **114**: 556–572.

Costa JE. 1988. Rheologic, geomorphic, and sedimentologic differentiation of water floods, hyperconcentrated flows, and debris flows. In *Flood Geomorphology*, Baker VR, Kochel RC, Patton PC (eds), Wiley: New York; 113–122.

De Haas T, Braat L, Leuven JFW, Lokhorst IR, Kleinhans MG. 2015a. The effect of debris-flow composition and topography on runout distance, depositional mechanisms and deposit morphology. *Journal of Geophysical Research: Earth Surface* **120**: 1949–1972.

De Haas T, Hauber E, Conway SJ, van Steijn H, Johnsson A, Kleinhans MG. 2015b. Earth-like aqueous debris-flow activity on Mars at high orbital obliquity in the last million years. *Nature Communications* **6:7543**. DOI: 10.1038/ncomms8543.

De Haas T, Kleinhans MG, Carbonneau PE, Rubensdotter L, Hauber E. 2015c. Surface morphology of fans in the high-Arctic periglacial environment of Svalbard: controls and processes. *Earth-Science Reviews* **146**: 163–182.

De Haas T, Ventra D, Hauber E, Conway SJ, Kleinhans MG. 2015d. Sedimentological analyses of Martian gullies: the subsurface as the key to the surface. *Icarus* **258**: 92–108.

De Haas T, van den Berg W, Braat L, Kleinhans MG. 2016. Autogenic avulsion, channelization and backfilling dynamics of debris-flow fans, Sedimentology. DOI: 10.1111.sed12275.

Dowling CA, Santi PM. 2014. Debris flows and their toll on human life: a global analysis of debris-flow fatalities from 1950 to 2011. *Natural Hazards* **71**: 203–227.

Egashira S, Honda N, Itoh T. 2001. Experimental study on the entrainment of bed material into debris flow. *Physics and Chemistry of the Earth, Part C* **26**: 645–650.

Fagents SA, Baloga SM. 2006. Toward a model for the bulking and debulking of lahars. *Journal of Geophysical Research: Solid Earth* **111**: B10201. DOI: 10.1029/2005JB003986.

Frank F, McArdell B, Huggel C, Vieli A. 2015. The importance of erosion for debris flow runout modelling from applications to the Swiss Alps. *Natural Hazards and Earth System Sciences Discussions* **3**: 2379–2417.

Griswold JP, Iverson RM. 2008. Mobility statistics and automated hazard mapping for debris flows and rock avalanches. *US Geological Survey Scientific Investigations Report* 2007–5276.

Guthrie R, Hockin A, Colquhoun L, Nagy T, Evans S, Ayles C. 2010. An examination of controls on debris flow mobility: evidence from coastal British Columbia. *Geomorphology* **114**: 601–613.

Han Z, Chen G, Li Y, He Y. 2015. Assessing entrainment of bed material in a debris-flow event: a theoretical approach incorporating Monte Carlo method. *Earth Surface Processes and Landforms* **40**: 1877–1890.

Hoffmans GJ, Pilarczyk KW. 1995. Local scour downstream of hydraulic structures. *Journal of Hydraulic Engineering* **121**: 326–340.

Hsu L, Dietrich WE, Sklar LS. 2008. Experimental study of bedrock erosion by granular flows. *Journal of Geophysical Research: Earth Surface* **113**: F02001. DOI: 10.1029/2007JF000778.

Hsu L, Dietrich W, Sklar L. 2014. Mean and fluctuating basal forces generated by granular flows: laboratory observations in a large vertically rotating drum. *Journal of Geophysical Research: Earth Surface* **119**: 1283–1309.

Hungr O, Morgan G, Kellerhals R. 1984. Quantitative analysis of debris torrent hazards for design of remedial measures. *Canadian Geotechnical Journal* **21**: 663–677.

Hungr O, McDougall S, Bovis M. 2005. Entrainment of material by debris flows. In *Debris-Flow Hazards and Related Phenomena*, Jakob M, Hungr O (eds), Springer: Berlin; 135–158.

Iverson RM. 1997. The physics of debris flows. *Reviews of Geophysics* **35**: 245–296.

Iverson RM. 2012. Elementary theory of bed-sediment entrainment by debris flows and avalanches. *Journal of Geophysical Research: Earth Surface* **117**: F03006. DOI: 10.1029/2011JF002189.

Iverson RM. 2014. Debris flows: behaviour and hazard assessment. *Geology Today* **30**: 15–20.

Iverson RM, Denlinger RP. 2001. Flow of variably fluidized granular masses across three-dimensional terrain. 1. Coulomb mixture theory. *Journal of Geophysical Research: Solid Earth* **106**: 537–552.

Iverson RM, Ouyang C. 2015. Entrainment of bed material by Earth-surface mass flows: review and reformulation of depth-integrated theory. *Reviews of Geophysics* **53**: 27–58.

Iverson RM, Logan M, LaHusen RG, Berti M. 2010. The perfect debris flow? Aggregated results from 28 large-scale experiments. *Journal of Geophysical Research: Earth Surface* **115**: F03005. DOI: 10.1029/2009JF001514.

Iverson RM, Reid ME, Logan M, LaHusen RG, Godt JW, Griswold JP. 2011. Positive feedback and momentum growth during debris-flow entrainment of wet bed sediment. *Nature Geoscience* **4**: 116–121.

Johnson C, Kokelaar B, Iverson R, Logan M, LaHusen R, Gray J. 2012. Grain-size segregation and levee formation in geophysical mass flows. *Journal of Geophysical Research: Earth Surface* **117**: F01032. DOI: 10.1029/2011JF002185.

Kaitna R, Dietrich W, Hsu L. 2014. Surface slopes, velocity profiles and fluid pressure in coarse-grained debris flows saturated with water and mud. *Journal of Fluid Mechanics* **741**: 377–403.

Mangeney A, Roche O, Hungr O, Mangold N, Faccanoni G, Lucas A. 2010. Erosion and mobility in granular collapse over sloping beds. *Journal of Geophysical Research: Earth Surface* **115**: F03040. DOI: 10.1029/2009JF001462.

McCoy S, Kean J, Coe J, Tucker G, Staley D, Wasklewicz T. 2012. Sediment entrainment by debris flows: in situ measurements from the headwaters of a steep catchment. *Journal of Geophysical Research: Earth Surface* **117**: F03016. DOI: 10.1029/2011JF002278.

Navratil O, Liébault F, Bellot H, Travaglini E, Theule J, Chambon G, Laigle D. 2013. High-frequency monitoring of debris-flow propagation along the Réal Torrent, Southern French Prealps. *Geomorphology* **201**: 157–171.

Okuda S, Suwa H. 1984. Some relationships between debris flow motion and micro-topography for the Kamikamihori fan, North Japan Alps. In *Catchment Experiments in Fluvial Geomorphology*, Geo Books: Norwich, UK; 447–464.

Pan H-l, Huang J-c, Ou G-q. 2015. Mechanism of downcutting erosion of debris flow over a movable bed. *Journal of Mountain Science* **12**: 243–250.

Pérez FL. 2001. Matrix granulometry of catastrophic debris flows (December 1999) in central coastal Venezuela. *Catena* **45**: 163–183.

Prancevic JP, Lamb MP, Fuller BM. 2014. Incipient sediment motion across the river to debris-flow transition. *Geology* **42**: 191–194.

Reid ME, Iverson RM, Logan M, LaHusen RG, Godt J, Griswold J. 2011. Entrainment of bed sediment by debris flows: results from large-scale experiments. In *Debris-Flow Hazards Mitigation, Mechanics, Prediction, and Assessment: Proceedings of 5th International Conference,* Padua, Italy; 367–374.

Rickenmann D. 1999. Empirical relationships for debris flows. *Natural Hazards* **19**: 47–77.

Rickenmann D. 2005. Runout prediction methods. In *Debris-Flow Hazards and Related Phenomena*, Jakob M, Hungr O (eds), Springer: Berlin; 305-324.

Rickenmann D, Weber D, Stepanov B. 2003. Erosion by debris flows in field and laboratory experiments. In *Debris-Flow Hazards Mitigation: Mechanics, Prediction, and Assessment: Proceedings of 5th International Conference,* Padua, Italy; 883–894.

Santi PM, Higgins JD, Cannon SH, Gartner JE. 2008. Sources of debris flow material in burned areas. *Geomorphology* **96**: 310–321.

Savage SB, Hutter K. 1989. The motion of a finite mass of granular material down a rough incline. *Journal of Fluid Mechanics* **199**: 177–215.

Schürch P, Densmore A, Rosser N, McArdell BW. 2011. A novel debris-flow fan evolution model based on debris flow monitoring and lidar topography. In *Debris-Flow Hazards Mitigation: Mechanics, Prediction, and Assessment: Proceedings of 5th International Conference,* Padua, Italy; 263–272.

Song C, Wang P, Makse HA. 2008. A phase diagram for jammed matter. *Nature* **453**: 629–632.

Stock JD, Dietrich WE. 2006. Erosion of steepland valleys by debris flows. *Geological Society of America Bulletin* **118**: 1125–1148.

Takahashi T. 1978. Mechanical aspects of debris flow. *American Society of Civil Engineers Proceedings, Journal of the Hydraulics Division* **104**: 1153–1169.

Takahashi T. 1981. Debris flow. *Annual Review of Fluid Mechanics* **13**: 57–77.

Takahashi T. 1991. *Debris Flow: Mechanics, Prediction and Countermeasures.* Taylor & Francis: London.

Takahashi T. 2009. A review of Japanese debris flow research. *International Journal of Erosion Control Engineering* **2**: 1–14.

Theule J, Liébault F, Laigle D, Loye A, Jaboyedoff M. 2015. Channel scour and fill by debris flows and bedload transport. *Geomorphology* **243**: 92–105.

Tognacca C, Bezzola G, Minor H. 2000. Threshold criterion for debris-flow initiation due to channel-bed failure. In *Proceedings of the 2nd International Conference on Debris Flow, Hazards and Mitigation*, Wieczorek GF (ed), Taipei, Taiwan. Balkema: Rotterdam; 89–97.

Yohannes B, Hsu L, Dietrich W, Hill K. 2012. Boundary stresses due to impacts from dry granular flows. *Journal of Geophysical Research: Earth Surface* **117**: F02027. DOI: 10.1029/2011JF002150.

Supporting information

Additional supporting information may be found in the online version of this article at the publisher's web site.